# Superconducting topological Dirac semimetals: P6/m-Si<sub>6</sub> and P6/m-NaSi<sub>6</sub>

Alex Taekyung Lee\*

Department of Applied Physics, Yale University, New Haven, Connecticut 06520, USA

Kyungwha Park Department of Physics, Virginia Tech, Blacksburg, Virginia 24061, USA

In-Ho Lee<sup>†</sup>

Korea Research Institute of Standards and Science, Daejeon 34113, Korea (Dated: April 3, 2023)

We theoretically propose that hexagonal silicon-based crystals, P6/m-Si<sub>6</sub> and P6/m-NaSi<sub>6</sub>, are topological Dirac semimetals with superconducting critical temperatures of 12 K and 13 K, respectively, at ambient pressure. Band inversion occurs with the Fu-Kane topological invariant  $\mathbb{Z}_2 = 1$ , even in the absence of spin-orbit coupling. The Dirac nodes protected by  $C_6$  crystal rotational symmetry remain gapless with spin-orbit coupling. Using first-principles calculations, we find pressure-induced topological phase transitions for P6/m-Si<sub>6</sub> and P6/m-NaSi<sub>6</sub> with critical external pressures of 11.5 GPa and 14.9 GPa, respectively. Above the critical pressures, the Dirac bands are gapped with  $\mathbb{Z}_2 = 0$ , while the superconducting states and the crystal symmetries are retained. Our results may shed light into a search for silicon-based topological materials with superconductivity.

#### I. Introduction

Semiconducting silicon becomes indispensable in electronics due to its versatile features such as the ease of electron or hole doping in a wide range, high-temperature stability, non toxicity, and natural abundance. It is not uncommon to modify phases of solids by varying crystal structures and/or applying external stimuli. There has been a great effort in fabricating silicon in different condensed matter phases, especially a superconducting phase. Some metallic silicon phases were proposed to be superconducting under high pressures [1–5]. For doped silicon clathrates and boron-doped cubic silicon, superconductivity was observed at ambient pressure [6-8]. Recently, hexagonal silicon-based crystals P6/m-Si<sub>6</sub> and P6/m-NaSi<sub>6</sub>, which can be synthesized similarly to Ref. 9, were predicted to show superconductivity (transition temperature of 12 K and 13 K, respectively) at ambient pressure [10].

Topology in the reciprocal space plays an important role in quantum materials properties due to topological protection. Based on symmetries, gapped and gapless quantum phases including a superconducting phase can be topologically classified [11]. For example, three-dimensional Dirac semimetals which can exist in the presence of time-reversal and inversion symmetries, are categorized into two classes [12]. In the first class, band inversion occurs with a nontrivial Fu-Kane  $\mathbb{Z}_2$  topological invariant [13] and associated Fermi arc surface states, and Dirac nodes are protected by crystal rotational symmetry [15, 44]. This class is henceforth referred to as a topological Dirac semimetal phase, following Ref. [12]. In

the second class, Dirac nodes are protected by nonsymmorphic space group [16] without band inversion.

Most topological materials are not based on silicon. A topological Dirac semimetal phase was discovered in a silicon-containing compound,  $\operatorname{CaAl_2Si_2}$  (space group No. 164, point group  $D_{3d}$ ) [17, 18] in the presence of spin-orbit coupling (SOC). Silicon-based crystals Cmcm-AHT-Si<sub>24</sub> and Cmcm-VFI-Si<sub>36</sub> have been proposed to be topological nodal line semimetals only when SOC is excluded [19]. With SOC, the nodal lines are gapped with a small energy gap of 1 meV [19].

Recently, superconductivity was observed in threedimensional topological Dirac semimetals such as Cd<sub>3</sub>As<sub>2</sub>[20–22], Au<sub>2</sub>Pb[23, 24], KZnBi[25], PdTe<sub>2</sub>[26, 27], and BaSn<sub>3</sub>[28]. To the best of our knowledge, siliconbased topological Dirac semimetals with superconductivity have not been proposed or synthesized yet. Superconductivity in topological Dirac semimetals is appealing considering the possibility to create odd-parity or spin-triplet Cooper pair interaction by doping and/or breaking time-reversal symmetry [29–31]. Furthermore, superconductors with a nontrivial Fu-Kane  $\mathbb{Z}_2$  topological invariant were proposed to be platforms for realization of Majorana zero modes [32] whose braiding is used for topological quantum computation [33, 34]. Families of superconductors with a nontrivial  $\mathbb{Z}_2$  invariant showed promising experimental signatures of Majorana zero modes at the ends of magnetic vortices [35, 36].

In this work, we propose that P6/m-Si<sub>6</sub> and P6/m-NaSi<sub>6</sub> are topological Dirac semimetals with superconductivity at ambient pressure even when SOC is included. We find that the silicon-based crystals undergo a topological phase transition driven by hydrostatic pressure without any structural changes. Above slightly different critical pressures, both silicon-based crystals become topologically trivial in the superconducting state.

 $<sup>^{*}</sup>$  neotechlee@gmail.com

<sup>†</sup> corresponding author ihlee@kriss.re.kr

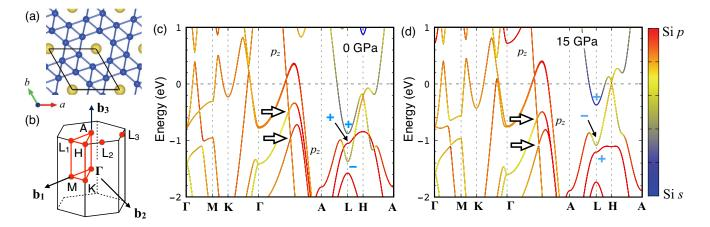


FIG. 1. (a) Top view of the atomic structure of P6/m-NaSi<sub>6</sub> with a unit cell. Isostructure P6/m-Si<sub>6</sub> can be obtained by removing Na atoms from P6/m-NaSi<sub>6</sub>. (b) First Brillouin zone for P6/m-Si<sub>6</sub> and P6/m-NaSi<sub>6</sub>. SOC-included DFT band structures of P6/m-Si<sub>6</sub> at (c) 0 GPa and (d) 15 GPa, where the Fermi level is set to zero. All bands are at least doubly degenerate. Relative proportions of Si s and p-orbital characters are encoded in colors. The Dirac points are indicated as arrows and the parity of a few occupied bands are shown.

#### II. Methods

We employ density functional theory (DFT) with projector augmented wave (PAW) [37] pseudopotentials and the Perdew-Burke-Ernzerhof generalized gradient approximation (PBE-GGA) [38] for the exchangecorrelation functional, as implemented in the VASP software [39]. A plane-wave basis set with a kinetic energy cutoff of 500 eV is used. We use  $\Gamma$ -centered k-point meshes of  $8 \times 8 \times 20$  for bulk P6/m-Si<sub>6</sub> and P6/m-NaSi<sub>6</sub> and  $8 \times 8 \times 1$  for finite slabs. Starting with the geometries from Ref. 10, we further optimize the atomic coordinates and lattice constants until the residual forces are less than 0.01 eV/Å with and without pressure. The optimized bulk hexagonal lattice parameters for P6/m- $Si_6 (P6/m-NaSi_6)$  are a = 6.81 (6.76) Å and c = 2.50(2.44) Å without pressure, which are close to those in Ref. 10. The relaxed atomic coordinates can be found in Appendix A.

We compute the Fu-Kane  $\mathbb{Z}_2$  topological invariant [13] from the parity of all valence or occupied bands at the time-reversal invariant momentum (TRIM) points as well as by using the Wilson loop method [40, 41]. To apply the Wilson loop method and to investigate the surface states, we first construct a tight-binding Hamiltonian for the Si s+p bands by generating 24 (33) maximally localized Wannier functions for P6/m-Si<sub>6</sub> (P6/m-NaSi<sub>6</sub>), using WANNIER90 code [42, 56] (see Appendix B). Then, we calculate the surface Green's function of the semi-infinite system based on the Wannier-function tight-binding model, using WannierTools code[41]. Irreducible representations of bands at the high symmetry  $\mathbf{k}$  points and along the  $\Gamma$ -A axis are obtained using Quantum Espresso [43].

#### III. Results and discussion

The atomic structure of P6/m-NaSi<sub>6</sub> (space group no. 175, point group  $C_{6h}$ ) is shown in Fig. 1(a), where the stacking along the c axis is identical for all atomic layers. The structure of P6/m-Si<sub>6</sub> is obtained by simply removing Na atoms from that of P6/m-NaSi<sub>6</sub>. (see Appendix A.) The Na atoms can be easily removed by the degassing process, since the migration barrier of Na atoms along the cylindrical holes is only 0.48 eV [10]. This barrier is 0.17 eV lower than that for the Cmcm phase [9].

Let us first discuss electronic and topological properties without pressure and then with pressure. Fig. 1(c) shows the electronic structure of P6/m-Si<sub>6</sub> at symmetric  ${\bf k}$  points with SOC in the absence of pressure. Mostly p-orbital character is dominant near the Fermi level. However, s-orbital character is locally dominant in the  $k_z=\pi/c$  plane, i.e., along the A-L-H-A lines. At the L point, bands at -0.86 eV and -1.04 eV (relative to the Fermi level) have strong s-orbital and  $p_z$ -orbital characters, respectively, while bands at -1.36 eV have characters of mixed s and  $p_x+p_y$  orbitals. (see Appendix C.) Strong Si p-orbital characteristics also appear in most of the  ${\bf k}$  space except for the  $k_z=\pi/c$  plane for P6/m-NaSi<sub>6</sub>, as presented in Fig. 2.

For P6/m-Si<sub>6</sub> at 0 GPa, the parity analysis at the TRIM points gives  $\mathbb{Z}_2 = 1$  (see Appendix B.) which results from the band inversion at the L points, as shown in Fig. 1(c). (Note that a unit cell of P6/m-Si<sub>6</sub> has 24 valence electrons.) At the L points, the 23th and 24th (25th and 26th) bands at -1.36 eV (-1.04 eV) have - (+) parity, as depicted in Fig. 1(c). The band inversion is not induced by SOC because  $\mathbb{Z}_2 = 1$  without SOC.

The analysis of irreducible representations at the L point indicates that the opposite parity for the two band

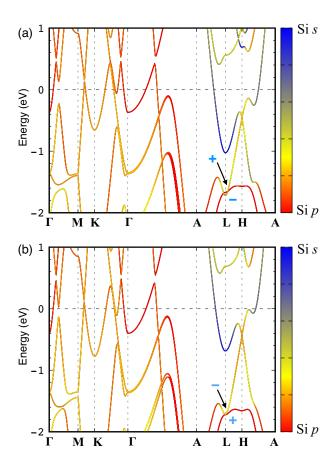


FIG. 2. Electronic band structure obtained from first-principles calculations using DFT. First-principles band structures of P6/m-NaSi<sub>6</sub> at pressure (a) 0 GPa and (b) 15 GPa, including spin-orbit coupling. According to the relative weight of the Si s character and the Si p character, the band color was encoded as shown in the legend. The band structure calculation at pressure 15 GPa shows the band structure just before band inversion occurs. The situation of band inversion that occurs with changes in pressure can be seen, especially in the L-H section.

pairs originates from the horizontal mirror symmetry  $\sigma_h$ . The irreducible representation and eigenvalues of  $\sigma_h$  of the bands at the L point are listed in Table I. The 23th/24th bands belong to irreducible representation  $B_u$  (where an eigenvalue of horizontal mirror reflection  $\sigma_h$  is +1), while the 25th/26th bands belong to irreducible representation  $B_g$  (where an eigenvalue of  $\sigma_h$  is -1). We also confirm that  $\mathbb{Z}_2 = 1$  using the Wilson loop method. (see Appendix B.) Even when the parity of all occupied bands below the Fermi level is counted, we find that  $\mathbb{Z}_2 = 1$  persists.

For P6/m-Si<sub>6</sub> with SOC in the absence of pressure, along the  $\Gamma$ -A direction, we find several possible band crossing points in the vicinity of the Fermi level. To identify gapless Dirac nodes, we zoom-in the bands near the crossing points with numerical accuracy of 10  $\mu$ eV, as shown in Fig. 3. The bands at i, ii, and iv are gapped

TABLE I. Irreducible representation (irrep), point group symmetries, and their eigenvalues of bands at L point, for P6/m-Si<sub>6</sub> at 0 GPa.  $C_2$  is two-fold rotation operator with respect to the z-axis. I and  $\sigma_h$  are two-fold inversion and horizontal mirror plane operators, respectively. The highest occupied band is 24th band.

band #	irrep	$C_2$	$\sigma_h$	I
1, 2	$B_u$	-1	+1	-1
3, 4	$A_g$	+1	+1	+1
5, 6	$B_g$	-1	-1	+1
7, 8	$B_u$	-1	+1	-1
9, 10	$A_u$	+1	-1	-1
11, 12	$A_g$	+1	+1	+1
13, 14	$B_g$	-1	-1	+1
15, 16	$A_u$	+1	-1	-1
17, 18	$B_u$	-1	+1	-1
19, 20	$A_g$	+1	+1	+1
21, 22	$A_u$	+1	-1	-1
23, 24	$B_u$	-1	+1	-1
25, 26	$B_g$	-1	-1	+1

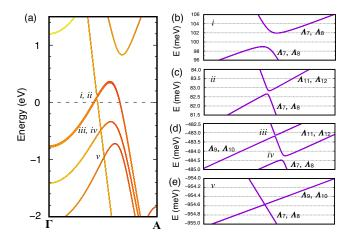


FIG. 3. SOC-included DFT bands for (a) P6/m-Si<sub>6</sub> at 0 GPa, between Γ and A. (b)-(e) enlarged bands near 5 possible band crossing points (i-v) for (a).  $\Lambda_i$  represent irreducible representations of double group  $C_6$  along the Γ-A direction. Points iii and v are gapless Dirac nodes (when  $\Lambda_{7,8}$  bands and  $\Lambda_{9,10}$  bands meet each other).

with 0.07-28.9 meV, while the crossing points iii and v are gapless within numerical accuracy. We also analyze irreducible representations  $\Lambda_i$  of the bands near the crossing points, considering that double group  $C_6$  is applied to the bands along the  $\Gamma$ -A direction. This symmetry analysis [Figs. 3(b)-(e)] agrees with the numerical result. The Dirac nodes along the  $k_z$  axis are protected by the crystal sixfold rotational symmetry  $C_6$ . The gapless protected Dirac nodes in conjunction with our analysis of the  $\mathbb{Z}_2$  invariant, suggest that P6/m-Si<sub>6</sub> is a topological Dirac semimetal.

For P6/m-NaSi<sub>6</sub>, it is tricky to compute the  $\mathbb{Z}_2$  in-

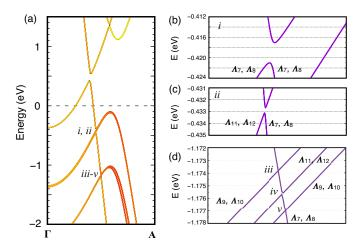


FIG. 4. (a) DFT bands in P6/m-NaSi<sub>6</sub> at 0 GPa, between  $\Gamma$  and A. (b)-(d) enlarged bands near 5 possible band crossing points (i-v) for (a). Points iii and v are gapless Dirac nodes (when  $\Lambda_{7,8}$  bands and  $\Lambda_{9,10}$  bands meet each other).

variant by counting the parity of N bands at the TRIM points, where N is the number of valence electrons, since N is now an odd number due to the Na atom. (In Ref. 13, each degenerate pair was counted only once for centrosymmetric metals.) In order to circumvent this, we take into account all occupied bands below the Fermi level at the TRIM points in our calculation of the  $\mathbb{Z}_2$ invariant. Note that there are different numbers of occupied bands at different TRIM points. For P6/m-NaSi<sub>6</sub> at 0 GPa, the product of the parity values of all occupied bands at each L point is positive, while the corresponding products at the other 5 TRIM points are negative. (See Appendix B.) This gives rise to  $\mathbb{Z}_2 = 1$  and the band inversion also occurs at the L points, as shown in Fig. 2(a). Therefore, similarly to P6/m-Si<sub>6</sub>, P6/m-NaSi<sub>6</sub> is also a topological Dirac semimetal. The gapless Dirac nodes [crossing points iii and v in Fig. 4(d)] are found below the Fermi level.

The nontrivial topology of three-dimensional Dirac bands in P6/m-Si<sub>6</sub> and P6/m-NaSi<sub>6</sub> indicates that there are nontrivial surface states. We calculate surface states using the surface Green's function of the semi-infinite system described earlier, considering two surface types: surfaces parallel and perpendicular to the  $\Gamma$ -A direction, *i.e.*, (100) and (001) surfaces, respectively. Fig. 5 shows the calculated local density of states which is an imaginary part of the surface Green's function, for the (100) and (001) surfaces. At the chemical potential, corresponding to one of the Dirac node energies, for the (100) surface, two arc-shaped (left and right sides of hourglass) surface states connect the two Dirac node projection points (with bulk characteristics) indicated as solid dots along the  $k_z$  axis in Fig. 5(b). This is expected because each Dirac node consists of degenerate Weyl nodes with opposite chirality in topological Dirac semimetals [44, 45].

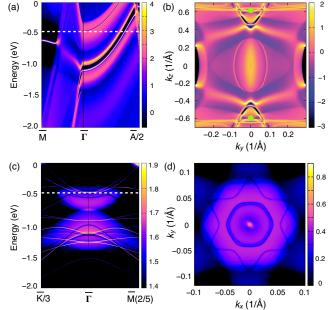


FIG. 5. Electronic structure or local density of states of surface states along the two-dimensional symmetric  $\mathbf{k}$  points (a,c), in the  $k_y$ - $k_z$  plane (b) and in the  $k_x$ - $k_y$  plane (d) for the semi-infinite (100) and (001) surfaces of P6/m-Si<sub>6</sub>, respectively. Horizontal dashed lines in (a) and (c) represent the Dirac point energies, respectively. Filled dots in (b) represent the projection points of the Dirac nodes onto the  $k_y$ - $k_z$  plane. In (a)-(d), bright color indicates higher density of states at the surface.

For the (001) surface, the surface states appear as a point [Fig. 5(d)]. In this case, the two Dirac nodes along the  $k_z$  axis are projected onto the same point, *i.e.*, the origin, in the  $k_x$ - $k_y$  plane. Thus, point-like surface states are expected rather than arc-shaped surface states. The features of the surface states for the (100) and (001) surfaces agree with those of prototype topological Dirac semimetals Na3Bi[44] and Cd<sub>3</sub>As<sub>2</sub>[15].

Now with pressure up to 15 GPa, the P6/m crystal symmetry is still maintained for P6/m-Si<sub>6</sub> and P6/m-NaSi<sub>6</sub>. Since the effect of pressure is similar for both crystals, as shown in Figs. 1 and 2, we mainly discuss P6/m-Si<sub>6</sub>. At 15 GPa, the amount of changes of the band structure depends on orbital characters. Specifically, the bands of s-orbital character are sensitive to pressure, while the bands of p-orbital character are somewhat rigid [Fig. 1(d)]. The band structure near the Fermi level changes significantly only in the  $k_z = \pi/c$  plane [Fig. 1(c) vs (d)]. At the L points, the s-orbital band is shifted by 0.51 eV, whereas the highest-energy occupied p-orbital band is shifted by 0.16 eV.

While the topological invariant is insensitive to small local perturbations such as disorder or impurities, pressure-induced deformation can be used to control the electronic structure [46–49]. For P6/m-Si<sub>6</sub>, under high pressure, the parity of the  $23 \, \text{th}/24 \, \text{th}$  bands is reversed

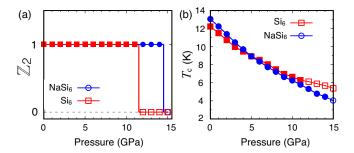


FIG. 6. (a)  $\mathbb{Z}_2$  topological invariants for P6/m-Si<sub>6</sub> and P6/m-NaSi<sub>6</sub> are shown as a function of external hydrostatic pressure. Critical external pressures of the topological phase transitions for P6/m-Si<sub>6</sub> and P6/m-NaSi<sub>6</sub> are 11.5 GPa and 14.9 GPa, respectively. (b) Superconducting critical temperatures  $T_c$  of P6/m-Si<sub>6</sub> and P6/m-NaSi<sub>6</sub>, obtained from Ref. 10 are shown as a function of external pressure. In (a) and (b), the filled (empty) symbols indicate the  $\mathbb{Z}_2 = 1$  ( $\mathbb{Z}_2 = 0$ ) phase.

to that of the 25th/26th bands at the L point [See the bands in the energy window between -1.4 and -1.0 eV in Fig. 1(d)], and so the bands with – parity become higher in energy than the bands with + parity, which removes the band inversion. This leads to a topological phase transition from nontrivial  $\mathbb{Z}_2 = 1$  to trivial  $\mathbb{Z}_2 = 0$ . The critical external pressure for the topological phase transition in P6/m-Si<sub>6</sub> is 11.5 GPa. [See Fig. 6(a).] The gapless Dirac nodes which exist below the critical pressure now open up a gap above the critical pressure, as shown in Fig. 1(d), due to the topological phase transition. In the case of P6/m-NaSi<sub>6</sub>, a similar topological phase transition occurs at 14.9 GPa, which is somewhat higher than the critical pressure of P6/m-Si<sub>6</sub>.

Theoretically, P6/m-Si<sub>6</sub> and P6/m-NaSi<sub>6</sub> were proposed to be superconductors at ambient pressure[10]. Fig. 6(b) shows the superconducting critical temperature  $T_c$  as a function of hydrostatic pressure. While  $T_c$  decreases monotonically as pressure (P) increases, both P6/m-Si<sub>6</sub> and P6/m-NaSi<sub>6</sub> are superconducting within the pressure range we consider,  $0 \le P \le 15$  GPa. Therefore, we propose that P6/m-Si<sub>6</sub> (P6/m-NaSi<sub>6</sub>) is a superconducting topological Dirac semimetal below 11.5 (14.9) GPa. We emphasize that P6/m-Si<sub>6</sub> and P6/m-NaSi<sub>6</sub> consist of light elements with atomic number 14 or less, based on silicon, in contrast to reported superconducting topological Dirac semimetals such as  $Cd_3As_2[20-22]$ ,  $Au_2Pb[23]$ , KZnBi[25],  $PdTe_2[26, 27]$ , and  $BaSn_3[28]$  which consist of heavy elements.

Due to the nesting vectors along  $k_z$ , it turns out that there is a modulation in Si-Si bond lengths (out-ofhexagonal plane) formed in the z direction. Indeed, we found a small oscillation of the out-of-plane bond length in the slab geometry. (see Appendix D.) The modulation is strongest on the surface and decreases near the center of the slab.

We calculated the Fermi surfaces from the two crys-

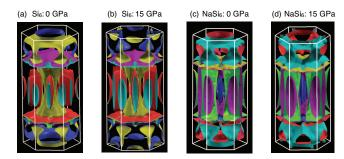


FIG. 7. Fermi surfaces of (a) P6/m-Si<sub>6</sub> at 0 GPa, (b) P6/m-Si<sub>6</sub> at 15 GPa, (c) P6/m-NaSi<sub>6</sub> at 0 GPa, and (d) P6/m-NaSi<sub>6</sub> at 150 GPa are shown, respectively. The Fermi surface is the surface of constant energy in the first BZ which separates occupied from unoccupied electron states at zero temperature. Electronic band structure obtained from first-principles calculations using DFT.

tal structures, P6/m-Si<sub>6</sub> and P6/m-NaSi<sub>6</sub>, as presented in Fig. 7. P6/m-Si<sub>6</sub> and P6/m-NaSi<sub>6</sub> can provide Dirac cones near or at the Fermi energy and show an anisotropic conducting channel due to their anisotropic bonding nature. Evidence of our proposed pressure-induced topological phase transition in P6/m-Si<sub>6</sub> and P6/m-NaSi<sub>6</sub> may be explored by transport experiments. The threedimensional Dirac nodes and resultant arc-shaped surface states are supposed to induce a unique field-direction dependence in Shubnikov-de Haas oscillations [50]. The chiral anomaly associated with Weyl nodes suggests the following interesting properties: (i) A large negative magnetoresistance is found when an external magnetic field is parallel to a current direction [51, 52]; (ii) Thermoelectric properties depends on the relative direction between an external magnetic field and a temperature gradient [53]; (iii) The giant planar Hall effect is expected when a current direction is not parallel to a magnetic field direction in plane [54, 55]. By measuring variations of the above properties upon external pressure, the proposed topological phase transition can be experimentally probed, similarly to Ref. 49.

#### IV. Conclusions

In summary, we have proposed that P6/m-Si<sub>6</sub> and P6/m-NaSi<sub>6</sub> crystals are superconducting topological Dirac semimetals at ambient pressure with  $\mathbb{Z}_2=1$ . The two gapless bulk Dirac nodes appear at -0.4832 eV and -0.9546 eV for the former and at -1.1740 eV and -1.1770 eV for the latter below the Fermi level. With hole doping, the Fermi level may be lowered to one of the two Dirac node energies for experimental signatures of the topological phase. The gapless Dirac nodes are protected by the crystal rotational symmetry in the presence of time-reversal symmetry. The topological Dirac semimetal phase for the crystals becomes topologically

trivial beyond a critical external pressure. This pressure-induced topological phase transition retains superconductivity and the original crystal symmetry group. The coexistence of a topological Dirac semimetal state and a superconducting state in the present crystals, along with a pressure-induced topological phase transition, will provide an interesting platform to study the interplay between topology in electronic structure and superconductivity.

ing Discovery Environment (XSEDE), which is supported by the National Science Foundation grant number ACI-1548562, by using computer time on the Comet supercomputer as enabled by XSEDE allocation MCA08X007. I.H.L was supported by the National Center for Materials Research Data (NCMRD) through the National Research Foundation of Korea (NRF) funded by the Ministry of Science and ICT (NRF-2021M3A7C2089748).

#### V. Acknowledgments

We thank Sohrab Ismail-Beigi for helpful discussions. This work also used the Extreme Science and Engineer-

- [1] W. Buckel and J. Wittig, Physics Letters 17, 187 (1965).
- [2] G. Stepanov, T. Valyanskaya, and E. Yakovlev, Sov. Phys.-Solid State (Engl. Transl.); (United States) 22 (1980).
- [3] G. Martinez, J. M. Mignot, G. Chouteau, K. J. Chang, M. M. Dacorogna, and M. L. Cohen, Physica Scripta T13, 226 (1986).
- [4] D. Erskine, P. Y. Yu, K. J. Chang, and M. L. Cohen, Phys. Rev. Lett. 57, 2741 (1986).
- [5] K. J. Chang, M. M. Dacorogna, M. L. Cohen, J. M. Mignot, G. Chouteau, and G. Martinez, Phys. Rev. Lett. 54, 2375 (1985).
- [6] H. Kawaji, H.-o. Horie, S. Yamanaka, and M. Ishikawa, Phys. Rev. Lett. 74, 1427 (1995).
- [7] D. Connétable, V. Timoshevskii, B. Masenelli, J. Beille, J. Marcus, B. Barbara, A. M. Saitta, G.-M. Rignanese, P. Mélinon, S. Yamanaka, and X. Blase, Phys. Rev. Lett. 91, 247001 (2003).
- [8] E. Bustarret, C. Marcenat, P. Achatz, J. Kačmarčik, F. Lévy, A. Huxley, L. Ortéga, E. Bourgeois, X. Blase, D. Débarre, and J. Boulmer, Nature 444, 465 (2006).
- [9] D. Y. Kim, S. Stefanoski, O. O. Kurakevych, and T. A. Strobel, Nature Materials 14, 169 (2015).
- [10] H.-J. Sung, W. H. Han, I.-H. Lee, and K. J. Chang, Phys. Rev. Lett. 120, 157001 (2018).
- [11] C.-K. Chiu, J. C. Y. Teo, A. P. Schnyder, and S. Ryu, Rev. Mod. Phys. 88, 035005 (2016).
- [12] B.-J. Yang and N. Nagaosa, Nature Communications 5, 4898 (2014).
- [13] L. Fu and C. L. Kane, Phys. Rev. B 76, 045302 (2007).
- [14] Z. Wang, Y. Sun, X.-Q. Chen, C. Franchini, G. Xu, H. Weng, X. Dai, and Z. Fang, Phys. Rev. B 85, 195320 (2012).
- [15] Z. Wang, H. Weng, Q. Wu, X. Dai, and Z. Fang, Phys. Rev. B 88, 125427 (2013).
- [16] S. M. Young, S. Zaheer, J. C. Y. Teo, C. L. Kane, E. J. Mele, and A. M. Rappe, Phys. Rev. Lett. 108, 140405 (2012).
- [17] H. Su, X. Shi, W. Xia, H. Wang, X. Hanli, Z. Yu, X. Wang, Z. Zou, N. Yu, W. Zhao, G. Xu, and Y. Guo, Phys. Rev. B 101, 205138 (2020).

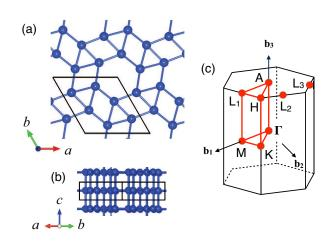
- [18] T. Deng, C. Chen, H. Su, J. He, A. Liang, S. Cui, H. Yang, C. Wang, K. Huang, C. Jozwiak, A. Bostwick, E. Rotenberg, D. Lu, M. Hashimoto, L. Yang, Z. Liu, Y. Guo, G. Xu, Z. Liu, and Y. Chen, Phys. Rev. B 102, 045106 (2020).
- [19] Z. Liu, H. Xin, L. Fu, Y. Liu, T. Song, X. Cui, G. Zhao, and J. Zhao, The Journal of Physical Chemistry Letters 10, 244 (2019), https://doi.org/10.1021/acs.jpclett.8b03345.
- [20] L. Aggarwal, A. Gaurav, G. S. Thakur, Z. Haque, A. K. Ganguli, and G. Sheet, Nature Materials 15, 32 (2016).
- [21] H. Wang, H. Wang, H. Liu, H. Lu, W. Yang, S. Jia, X.-J. Liu, X. C. Xie, J. Wei, and J. Wang, Nature Materials 15, 38 (2016).
- [22] C. Huang, B. T. Zhou, H. Zhang, B. Yang, R. Liu, H. Wang, Y. Wan, K. Huang, Z. Liao, E. Zhang, S. Liu, Q. Deng, Y. Chen, X. Han, J. Zou, X. Lin, Z. Han, Y. Wang, K. T. Law, and F. Xiu, Nature Communications 10, 2217 (2019).
- [23] L. M. Schoop, L. S. Xie, R. Chen, Q. D. Gibson, S. H. Lapidus, I. Kimchi, M. Hirschberger, N. Haldolaarachchige, M. N. Ali, C. A. Belvin, T. Liang, J. B. Neaton, N. P. Ong, A. Vishwanath, and R. J. Cava, Phys. Rev. B 91, 214517 (2015).
- [24] Y. Xing, H. Wang, C.-K. Li, X. Zhang, J. Liu, Y. Zhang, J. Luo, Z. Wang, Y. Wang, L. Ling, M. Tian, S. Jia, J. Feng, X.-J. Liu, J. Wei, and J. Wang, npj Quantum Materials 1, 16005 (2016).
- [25] J. Song, S. Kim, Y. Kim, H. Fu, J. Koo, Z. Wang, G. Lee, J. Lee, S. H. Oh, J. Bang, T. Matsushita, N. Wada, H. Ikegami, J. D. Denlinger, Y. H. Lee, B. Yan, Y. Kim, and S. W. Kim, Phys. Rev. X 11, 021065 (2021).
- [26] S. Teknowijoyo, N. H. Jo, M. S. Scheurer, M. A. Tanatar, K. Cho, S. L. Bud'ko, P. P. Orth, P. C. Canfield, and R. Prozorov, Phys. Rev. B 98, 024508 (2018).
- [27] Amit and Y. Singh, Phys. Rev. B 97, 054515 (2018).
- [28] K. Huang, A. Y. Luo, C. Chen, G. N. Zhang, X. L. Liu, Y. W. Li, F. Wu, S. T. Cui, Z. Sun, C. Jozwiak, A. Bostwick, E. Rotenberg, H. F. Yang, L. X. Yang, G. Xu, Y. F. Guo, Z. K. Liu, and Y. L. Chen, Phys. Rev. B 103, 155148 (2021).

- [29] S. Kobayashi and M. Sato, Phys. Rev. Lett. 115, 187001 (2015).
- [30] T. Hashimoto, S. Kobayashi, Y. Tanaka, and M. Sato, Phys. Rev. B 94, 014510 (2016).
- [31] M. Sato and Y. Ando, Reports on Progress in Physics 80, 076501 (2017).
- [32] J. Alicea, Rep. Prog. Phys. **75**, 076501 (2012).
- [33] A. Kitaev, Annals of Physics 303, 2 (2003).
- [34] S. D. Sarma, M. Freedman, and C. Nayak, npj Quantum Information 1, 15001 (2015).
- [35] A. Kreisel, P. J. Hirschfeld, and B. M. Andersen, Symmetry 12 (2020), 10.3390/sym12091402.
- [36] L. Kong, L. Cao, S. Zhu, M. Papaj, G. Dai, G. Li, P. Fan, W. Liu, F. Yang, X. Wang, S. Du, C. Jin, L. Fu, H.-J. Gao, and H. Ding, Nature Communications 12, 4146 (2021).
- [37] P. E. Blöchl, Phys. Rev. B **50**, 17953 (1994).
- [38] J. P. Perdew, K. Burke, and M. Ernzerhof, Phys. Rev. Lett. 77, 3865 (1996).
- [39] G. Kresse and D. Joubert, Phys. Rev. B 59, 1758 (1999).
- [40] A. A. Soluyanov and D. Vanderbilt, Phys. Rev. B 83, 035108 (2011).
- [41] Q. Wu, S. Zhang, H.-F. Song, M. Troyer, and A. A. Soluyanov, Computer Physics Communications 224, 405 (2018).
- [42] N. Marzari, A. A. Mostofi, J. R. Yates, I. Souza, and D. Vanderbilt, Rev. Mod. Phys. 84, 1419 (2012).
- [43] P. Giannozzi, O. Andreussi, T. Brumme, O. Bunau, M. B. Nardelli, M. Calandra, R. Car, C. Cavazzoni, D. Ceresoli, M. Cococcioni, N. Colonna, I. Carnimeo, A. D. Corso, S. de Gironcoli, P. Delugas, R. A. D. Jr, A. Ferretti, A. Floris, G. Fratesi, G. Fugallo, R. Gebauer, U. Gerstmann, F. Giustino, T. Gorni, J. Jia, M. Kawamura, H.-Y. Ko, A. Kokalj, E. Küçükbenli, M. Lazzeri, M. Marsili, N. Marzari, F. Mauri, N. L. Nguyen, H.-V. Nguyen, A. O. de-la Roza, L. Paulatto, S. Poncé, D. Rocca, R. Sabatini, B. Santra, M. Schlipf, A. P. Seitsonen, A. Smogunov, I. Timrov, T. Thonhauser, P. Umari, N. Vast, X. Wu, and S. Baroni, Journal of Physics: Condensed Matter 29, 465901 (2017).
- [44] Z. Wang, Y. Sun, X.-Q. Chen, C. Franchini, G. Xu, H. Weng, X. Dai, and Z. Fang, Phys. Rev. B 85, 195320 (2012).
- [45] J. W. Villanova, E. Barnes, and K. Park, Nano Letters 17, 963 (2017).
- [46] S. M. Young, S. Chowdhury, E. J. Walter, E. J. Mele, C. L. Kane, and A. M. Rappe, Phys. Rev. B 84, 085106 (2011).
- [47] M. S. Bahramy, B.-J. Yang, R. Arita, and N. Nagaosa, Nature Communications 3, 679 (2012).
- [48] A. Bansil, H. Lin, and T. Das, Rev. Mod. Phys. 88, 021004 (2016).
- [49] T. Ideue, M. Hirayama, Η. Taiko, T. Taka-S. hashi, Μ. Murase, Т. Miyake, Murakami. T. Y. Sasagawa, and Iwasa, Proceedings of the National Academy of Sciences 116, 25530F(2019), (a) Top view and (b) side view of the atomic struchttps://www.pnas.org/content/116/51/25530.full.pdf.
- [50] P. J. W. Moll, N. L. Nair, T. Helm, A. C. Potter, I. Kimchi, A. Vishwanath, and J. G. Analytis, Nature 535, 266 (2016).
- [51] A. A. Burkov, M. D. Hook, and L. Balents, Phys. Rev. B 84, 235126 (2011).
- [52] J. Xiong, S. K. Kushwaha, T. Liang, J. W. Krizan, M. Hirschberger, W. Wang, R. J.

- Cava, and N. P. Ong, Science **350**, 413 (2015), https://www.science.org/doi/pdf/10.1126/science.aac6089.
- [53] Z. Jia, C. Li, X. Li, J. Shi, Z. Liao, D. Yu, and X. Wu, Nature Communications 7, 13013 (2016).
- [54] A. A. Burkov, Phys. Rev. B 96, 041110 (2017).
- [55] M. Wu, G. Zheng, W. Chu, Y. Liu, W. Gao, H. Zhang, J. Lu, Y. Han, J. Zhou, W. Ning, and M. Tian, Phys. Rev. B 98, 161110 (2018).
- [56] G. Pizzi, V. Vitale, R. Arita, S. Blügel, F. Freimuth, G. Géranton, M. Gibertini, D. Gresch, C. Johnson, T. Koretsune, J. Ibañez-Azpiroz, H. Lee, J.-M. Lihm, D. Marchand, A. Marrazzo, Y. Mokrousov, J. I. Mustafa, Y. Nohara, Y. Nomura, L. Paulatto, S. Poncé, T. Ponweiser, J. Qiao, F. Thöle, S. S. Tsirkin, M. Wierzbowska, N. Marzari, D. Vanderbilt, I. Souza, A. A. Mostofi, and J. R. Yates, Journal of Physics: Condensed Matter 32, 165902 (2020).

## A. Atomic structure of P6/m-Si<sub>6</sub>

Fig. 8 shows the atomic structure of P6/m-Si<sub>6</sub>, which can be obtained by removing Na atoms from P6/m-NaSi<sub>6</sub>. In Table II, we provide the information of the atomic structure including lattice parameters and atomic coordinate. Note that all the structures have P6/m space group symmetry, at both 0 GPa and 15 GPa.



of  $16_{01}$  (a) Top view and (b) side view of the atomic structure of P6/m-Si<sub>6</sub>. (c) First Brillouin zone (BZ) of P6/m-Si<sub>6</sub>.  $\Gamma$ , M, A, and L points are time reversal invariant momentum points, which are related to  $\mathbb{Z}_2$  topological invariant calculation especially for crystals with inversion symmetry. P6/m (space group no. 175) is belong to the hexagonal Bravais lattice crystal system. The space group no. 175 has inversion symmetry.

TABLE II. Optimized lattice parameters and atomic coordinates of P6/m-Si<sub>6</sub> and P6/m-NaSi<sub>6</sub> phases at external pressure (P) of 0 GPa and 15 GPa, obtained from first-principles calculations using density-functional theory (DFT). Both P6/m-NaSi<sub>6</sub> and P6/m-Si<sub>6</sub> phases are hexagonal with  $\alpha = \beta = 90^{\circ}$ , and  $\gamma = 120^{\circ}$ .

Material	P (GPa)	a = b  (Å)	c (Å)	Atom	x	y	$\overline{z}$
P6/m-Si <sub>6</sub>	0	6.813	2.501	Si (6j)	0.154	0.733	0
P6/m-Si <sub>6</sub>	15	6.542	2.402	Si(6j)	0.145	0.725	0
P6/m-NaSi <sub>6</sub>	0	6.755	2.444	Na(1b)	0	0	0.5
,				Si(6j)	0.145	0.710	0
P6/m-NaSi <sub>6</sub>	15	6.536	2.377	Na(1b)	0	0	0.5
,				Si $(6j)$	0.144	0.713	0

#### B. $\mathbb{Z}_2$ topological invariant calculations

The topological phase of band structure can be classified by calculating topological invariant. We check the  $Z_2$  topology by calculating the parities at time-reversal invariant momenta, as shown in Table III, and using the hybrid Wannier charge center flow technique, which is equivalent to the Wilson loop method. To investigate the topological nature of the electronic states, we obtained maximally localized Wannier functions using the WANNIER90 code [42, 56] (see Fig. 9) and performed hybrid Wannier charge center flow calculations. With this Wannier model, the symmetry properties and  $\mathbb{Z}_2$  topological invariant could be directly computed.  $\mathbb{Z}_2$  topological invariants were calculated by observing hybrid Wannier charge center flows. The topological surface states were calculated using the Green's function approach, as implemented in the WannierTools code [41].

Space group no. 175 (P6/m, hexagonal) has inversion symmetry. Because of the existence of inversion symmetry in both P6/m-Si<sub>6</sub> and P6/m-NaSi<sub>6</sub>, the Fu-Kane parity criterion can be used to easily calculate the  $\mathbb{Z}_2$  topological invariants. We were able to obtain the same  $\mathbb{Z}_2$  topological invariants for both P6/m-Si<sub>6</sub> and P6/m-NaSi<sub>6</sub> by using two different methods, observing hybrid Wannier charge center flows and investigating Fu-Kane parity criterion.  $\nu_0$  is the strong topological index.  $\nu'_n$  (n=1,2,3) are weak topological indices. Table IV show the example for P6/m-Si<sub>6</sub> at 0 GPa. From the hybrid

TABLE III. Parities at time-reversal invariant momentum points of P6/m-Si<sub>6</sub> and P6/m-NaSi<sub>6</sub> at 0 GPa and 15 GPa.

		P6/	P6/m-Si <sub>6</sub>		-NaSi <sub>6</sub>
	$\mathbf{k}$ -point	0 GPa	15 GPa	0 GPa	15 GPa
Γ	(0,0,0)	+	+	_	_
$M_1$	(0.5, 0, 0)	+	+	_	_
$M_2$	(0, 0.5, 0)	+	+	_	_
A	(0, 0, 0.5)	+	+	_	_
$M_3$	(0.5, 0.5, 0)	+	+	_	_
$L_1$	(0.5, 0, 0.5)	_	+	+	_
$L_2$	(0, 0.5, 0.5)	_	+	+	_
$L_3$	(0.5, 0.5, 0.5)	_	+	+	_

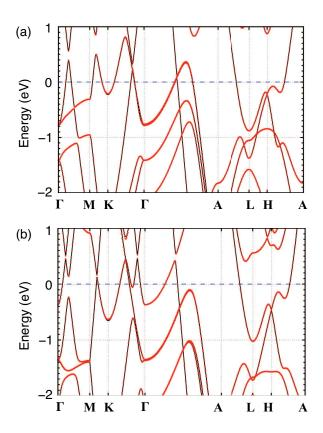


FIG. 9. First-principles bands (solid line) and Wannier bands (red filled circles) of P6/m-Si<sub>6</sub> at (a) 0 GPa and (b) 15 GPa. In the eV energy scale, there are no visible differences between two different bands. Spin-orbit coupling is included.

Wannier charge center flow calculations, we calculated  $\nu'_n$  (n = 1, 2, 3).  $\nu_0$  is obtained by

$$\nu_0 = \nu_1 + \nu_1' = \nu_2 + \nu_2' = \nu_3 + \nu_3' \mod 2$$
, (S1)

and thus we have  $(\nu_0; \nu_1'\nu_2'\nu_3') = (1;001)$ . Therefore, P6/m-Si<sub>6</sub> at 0 GPa has a strong topological nature. Similarly, we find that P6/m-NaSi<sub>6</sub> at 0 GPa has a strong topological nature.

TABLE IV.  $\nu_0$  and  $\nu'_n$  (n = 1, 2, 3) for P6/m-Si<sub>6</sub> obtained from hybrid Wannier charge center flow calculations, and correspond  $\{k_n\}$  points and **k**-planes.

$k_n$	k-plane	ν	
$k_1 = 0.0$	$k_2$ - $k_3$ plane	$\nu_1$ =1	
$k_1 = 0.5$	$k_2$ - $k_3$ plane	$\nu_1' = 0$	
$k_2 = 0.0$	$k_1$ - $k_3$ plane	$\nu_2 = 1$	
$k_2 = 0.5$	$k_1$ - $k_3$ plane	$\nu_2'=0$	
$k_3 = 0.0$	$k_1$ - $k_2$ plane	$\nu_3=0$	
$k_3 = 0.5$	$k_1$ - $k_2$ plane	$\nu_3'{=}1$	

## C. Band structures of P6/m-NaSi<sub>6</sub> and P6/m-Si<sub>6</sub>

In Fig. 10, we present the the weight of in-plane Si p character  $(p_x+p_y)$  and out-of-plane Si p character  $(p_z)$  on the band structure of P6/m-Si<sub>6</sub>. At 0 GPa,  $p_z$ -dominant band is higher in energy than the  $p_x+p_y$  band along the L-H-A interval, whereas the  $p_x+p_y$  band has lower energy than the  $p_z$  band at 15 GPa.

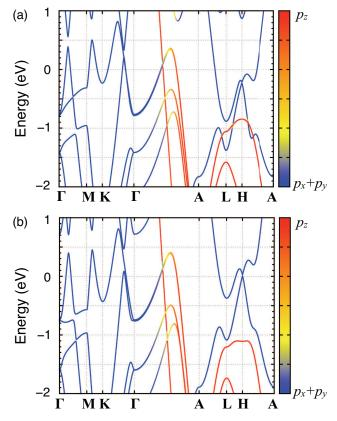


FIG. 10. Electronic band structure obtained from first-principles calculations using DFT. In the presence of SOC, band structures of P6/m-Si<sub>6</sub> at (a) 0 GPa and (b) 15 GPa and their projections on the the Si p character are shown. According to the relative weight of in-plane Si p character ( $p_x + p_y$ ) and out-of-plane Si p character ( $p_z$ ) the band colors were encoded as shown in the legend. The situation of band inversion that occurs with changes in external pressure (> 11.5 GPa) can be seen, especially in the L-H-A interval.

D. Si-Si bond lengths in the slab geometry

In Fig. 11, we plot the Si-Si bond length along the z direction (out of plane from the hexagonal surface). Note that the bond length distribution has an oscillation, while the oscillation of the bond length is largest and decreases near the bulk-like region.

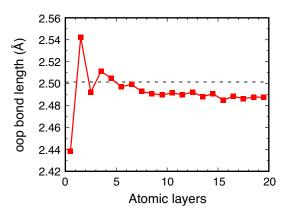
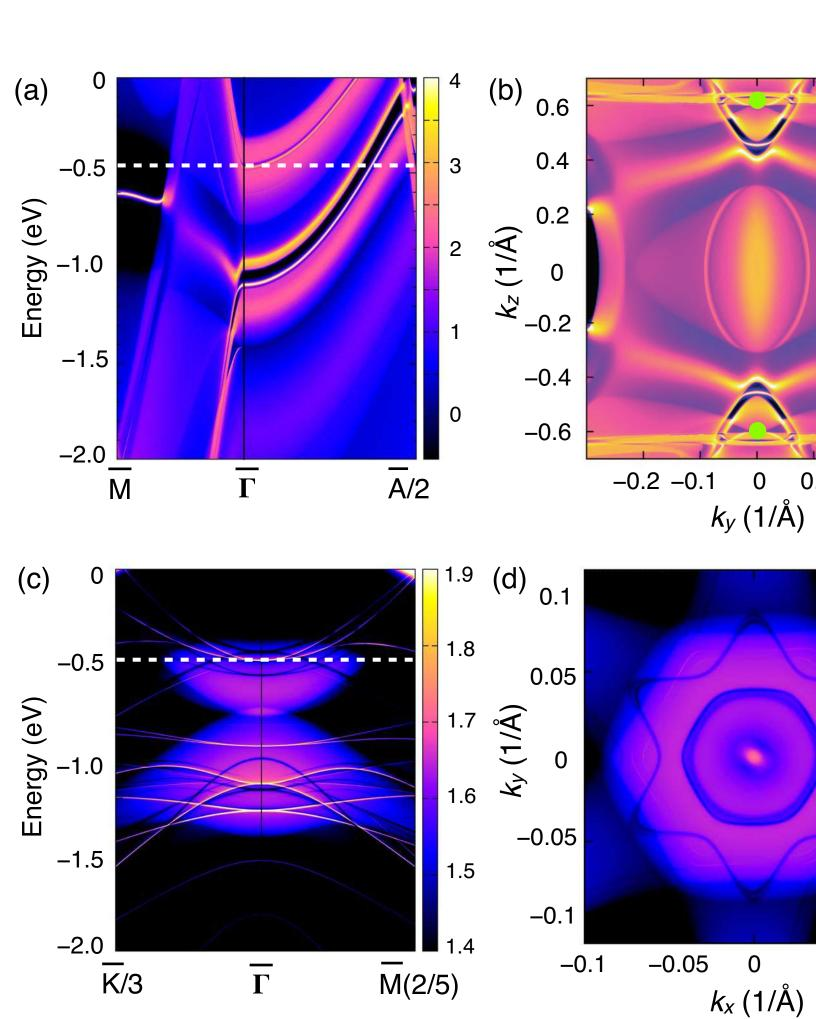
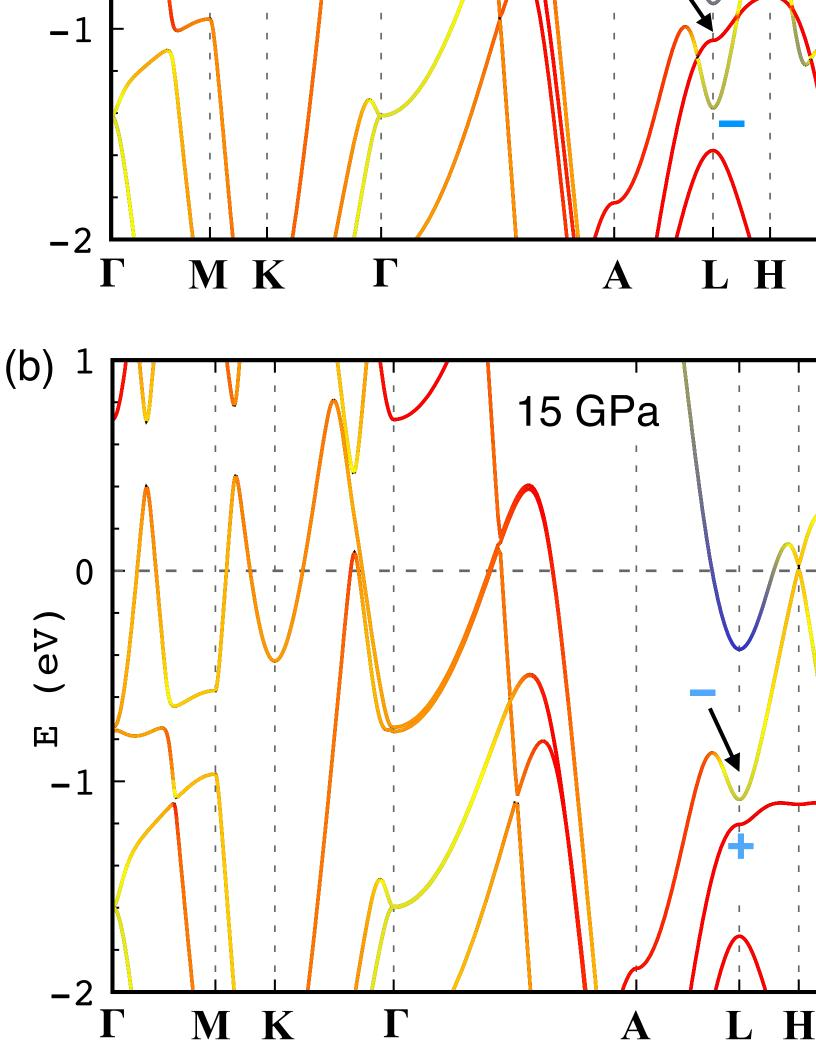
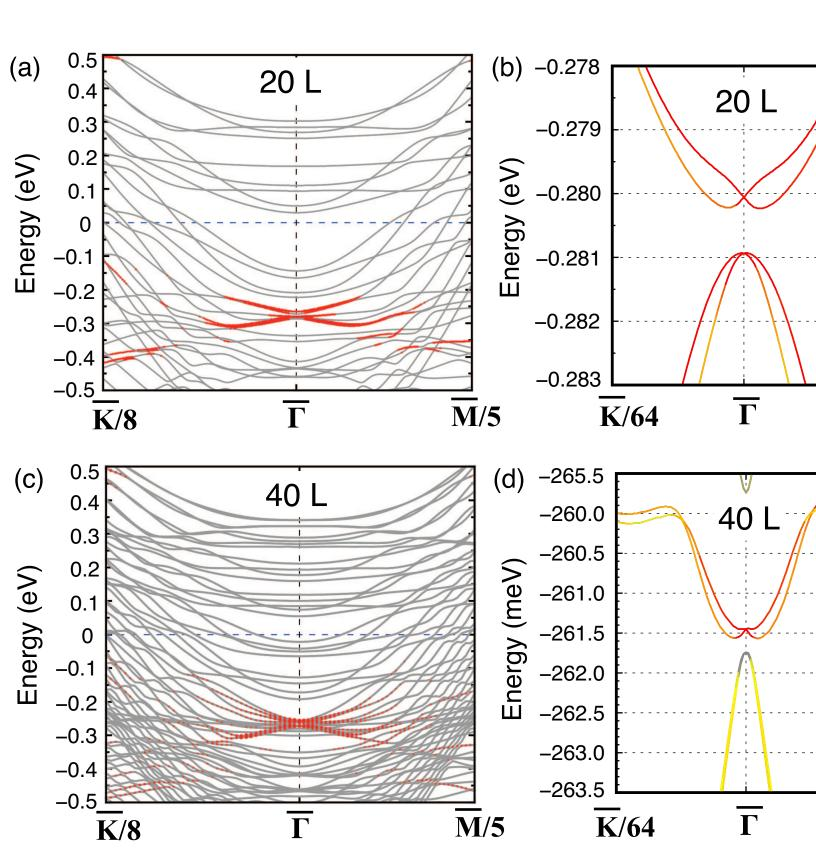
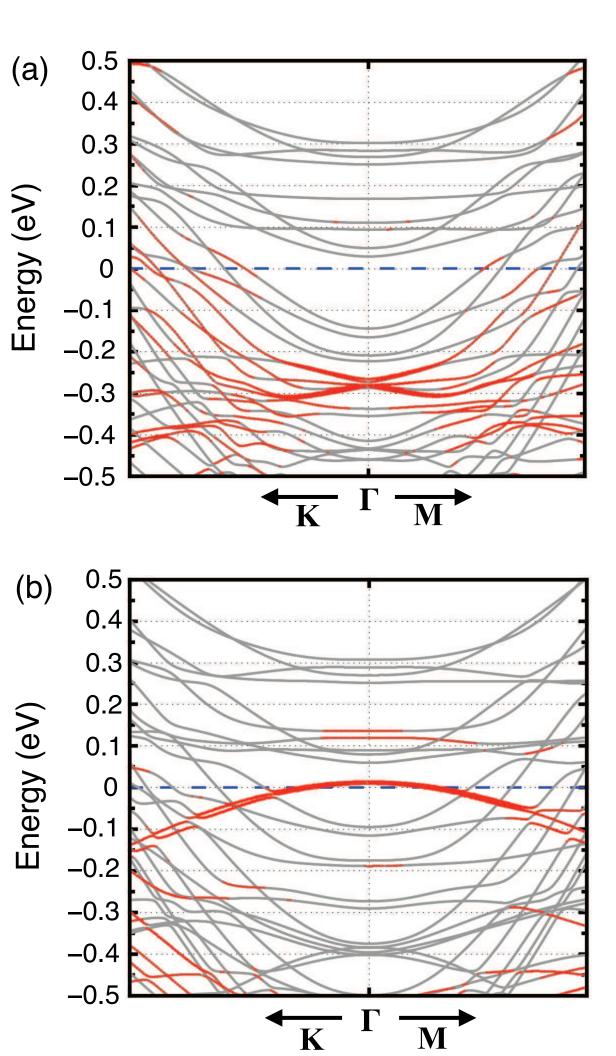


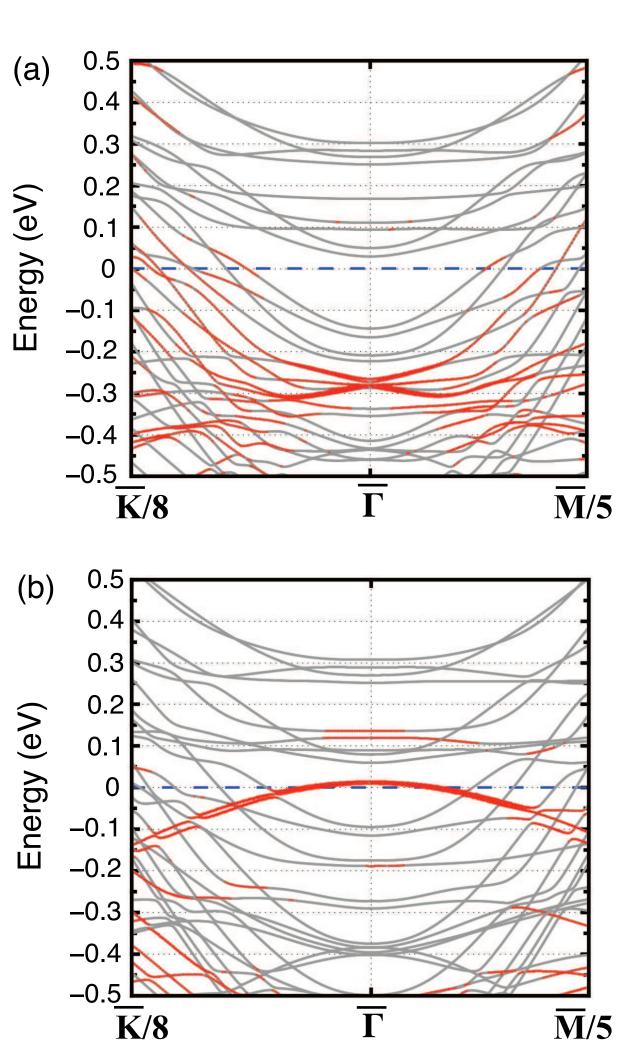
FIG. 11. Si-Si bond lengths, formed in the z direction also denoted by out-of-plane (oop bond lengths) from the hexagonal plane, in the relaxed 40-layer P6/m-Si<sub>6</sub> slab are shown. Position of the surface along the out-of-plane, is set to be zero. Dashed line represents the Si-Si bond length in the unrelaxed slab.

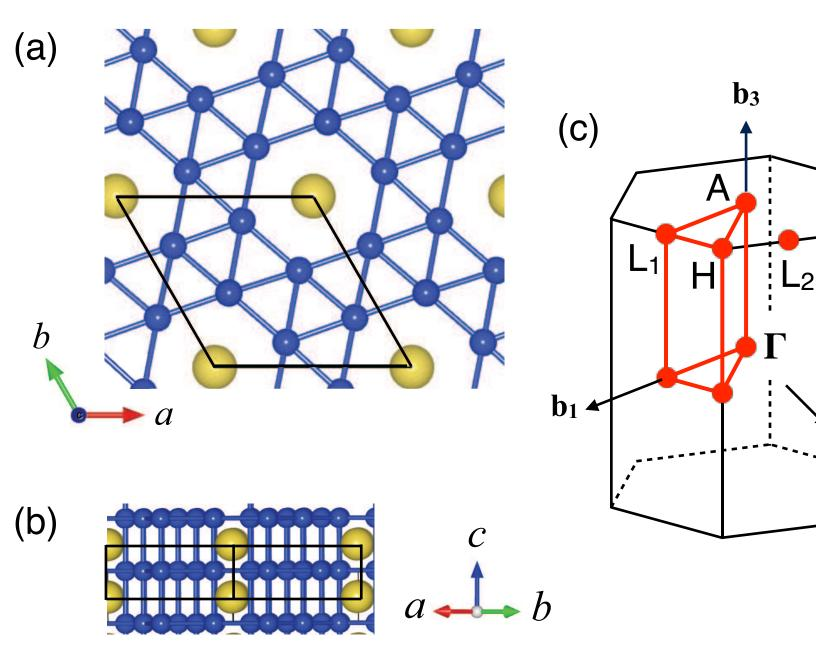


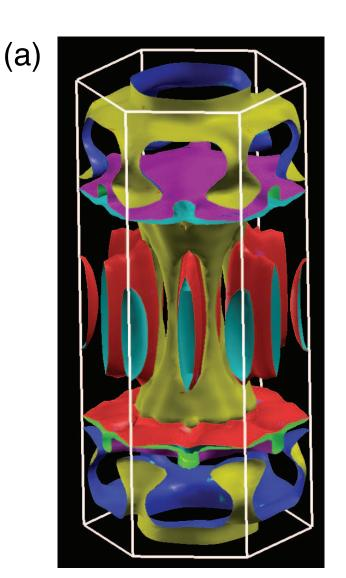




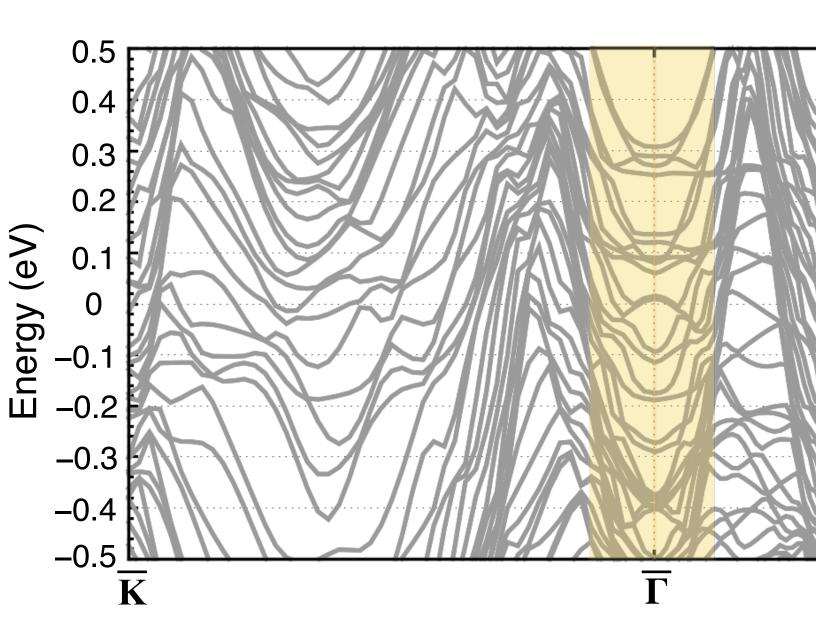












# Supplemental Material

Superconducting Dirac semimetals: P6/m-Si<sub>6</sub> and P6/m-NaSi<sub>6</sub>

Alex Taekyung Lee, 1, \* Kyungwha Park, 2, † and In-Ho Lee<sup>3,‡</sup>

<sup>1</sup>Department of Applied Physics, Yale University, New Haven, Connecticut 06520, USA

<sup>2</sup>Department of Physics, Virginia Tech, Blacksburg, Virginia 24060, USA

<sup>3</sup>Korea Research Institute of Standards and Science, Daejeon 34113, Korea

(Dated: April 3, 2023)

<sup>\*</sup> neotechlee@gmail.com

 $<sup>^{\</sup>dagger}$ kyungwha@vt.edu

<sup>&</sup>lt;sup>‡</sup> corresponding author ihlee@kriss.re.kr

## CONTENTS

I.	Atomic structure of $P6/m$ -Si <sub>6</sub>	2
II.	Band structures of $P6/m$ -NaSi <sub>6</sub> and $P6/m$ -Si <sub>6</sub>	3
III.	$\mathbb{Z}_2$ topological invariant calculations	4
IV.	Si-Si bond lengths in the slab geometry	6
V.	Fermi surfaces for $P6/m$ -Si <sub>6</sub> and $P6/m$ -NaSi <sub>6</sub>	7

# I. ATOMIC STRUCTURE OF P6/m-Si<sub>6</sub>

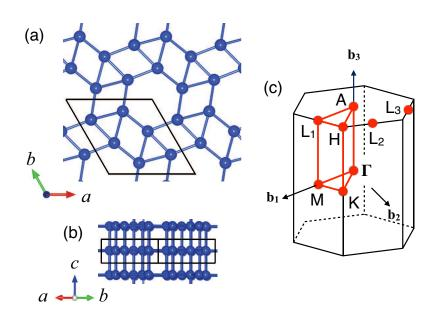


FIG. S1. (a) Top view and (b) side view of the atomic structure of P6/m-Si<sub>6</sub>. P6/m-Si<sub>6</sub> can be obtained by removing Na atoms from P6/m-NaSi<sub>6</sub>. (c) First Brillouin zone (BZ) of P6/m-Si<sub>6</sub>.  $\Gamma$ , M, A, and L points are time reversal invariant momentum points, which are related to  $\mathbb{Z}_2$  topological invariant calculation especially for crystals with inversion symmetry. P6/m (space group no. 175) is belong to the hexagonal Bravais lattice crystal system. The space group no. 175 has inversion symmetry.

TABLE S1. Optimized lattice parameters and atomic coordinates of P6/m-Si<sub>6</sub> and P6/m-NaSi<sub>6</sub> phases at external pressure of 0 GPa and 15 GPa, obtained from first-principles calculations using density-functional theory (DFT). Both P6/m-NaSi<sub>6</sub> and P6/m-Si<sub>6</sub> phases are hexagonal with  $\alpha = \beta = 90^{\circ}$ , and  $\gamma = 120^{\circ}$ .

Material	pressure (GPa)	a = b  (Å)	c (Å)	Atom	x	y	z
P6/m-Si <sub>6</sub>	0	6.813	2.501	Si (6j)	0.154	0.733	0
P6/m-Si <sub>6</sub>	15	6.542	2.402	Si(6j)	0.145	0.725	0
P6/m-NaSi <sub>6</sub>	0	6.755	2.444	Na(1b)	0	0	0.5
				Si(6j)	0.145	0.710	0
P6/m-NaSi <sub>6</sub>	15	6.536	2.377	Na(1b)	0	0	0.5
•				Si(6j)	0.144	0.713	0

# II. BAND STRUCTURES OF P6/m-NaSi<sub>6</sub> AND P6/m-Si<sub>6</sub>

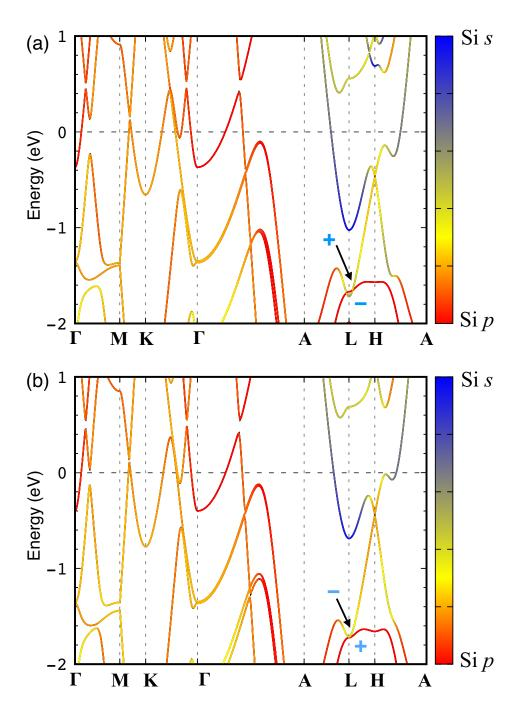


FIG. S2. Electronic band structure obtained from first-principles calculations using DFT. First-principles band structures of P6/m-NaSi<sub>6</sub> at pressure (a) 0 GPa and (b) 15 GPa, including spin-orbit coupling. According to the relative weight of the Si s character and the Si p character, the band color was encoded as shown in the legend. The band structure calculation at pressure 15 GPa shows the band structure just before band inversion occurs. The situation of band inversion that occurs with changes in pressure can be seen, especially in the L-H section.

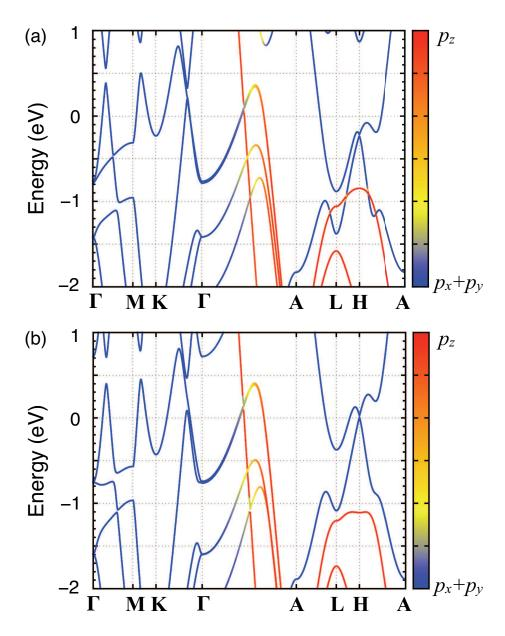


FIG. S3. Electronic band structure obtained from first-principles calculations using DFT. In the presence of SOC, band structures of P6/m-Si<sub>6</sub> at (a) 0 GPa and (b) 15 GPa and their projections on the the Si p character are shown. According to the relative weight of in-plane Si p character ( $p_x + p_y$ ) and out-of-plane Si p character ( $p_z$ ) the band colors were encoded as shown in the legend. The situation of band inversion that occurs with changes in external pressure (> 11.5 GPa) can be seen, especially in the L-H-A interval.

# III. $\mathbb{Z}_2$ TOPOLOGICAL INVARIANT CALCULATIONS

The topological phase of band structure can be classified by calculating topological invariant. The hybrid Wannier charge center flow technique, which is equivalent to the Wilson loop method. To investigate the topological nature of the electronic states, we obtained maximally localized Wannier functions using the WANNIER90 code [?] and performed hybrid Wannier charge center flow calculations. With this Wannier model, the symmetry properties and  $\mathbb{Z}_2$  topological invariant could be directly computed.  $\mathbb{Z}_2$  topological invariants were calculated by observing hybrid Wannier charge center flows. The topological surface states were calculated using the Green's function approach, as implemented in the WannierTools code [?].

Space group no. 175 (P6/m, hexagonal) has inversion symmetry. Because of the existence of inversion symmetry

TABLE S2	Parities at time-reversa	invariant momentum	points of P6/m-Sic an	nd P6/m-NaSie at 0 GPa	and 15 GPa
TADLE 52.	i allues at time-reversa.	. mvariani momenium	DOING OF 1 0/110-016 at	iu <i>i u/iii</i> -inasia at u Gi a	and 10 Gra.

		P6/m-Si <sub>6</sub>		P6/m-NaSi <sub>6</sub>	
	$\mathbf{k}$ -point	0 GPa	15 GPa	0 GPa	15 GPa
Γ	(0,0,0)	+	+	_	_
$M_1$	(0.5, 0, 0)	+	+	_	_
$M_2$	(0, 0.5, 0)	+	+	_	_
A	(0, 0, 0.5)	+	+	-	_
$M_3$	(0.5, 0.5, 0)	+	+	-	_
$L_1$	(0.5, 0, 0.5)	_	+	+	_
$L_2$	(0, 0.5, 0.5)	_	+	+	_
$L_3$	(0.5, 0.5, 0.5)	_	+	+	_

TABLE S3.  $\nu_0$  and  $\nu'_n$  (n=1,2,3) for P6/m-Si<sub>6</sub> obtained from hybrid Wannier charge center flow calculations, and correspond  $\{k_n\}$  points and **k**-planes.

$k_n$	k-plane	ν	
$k_1 = 0.0$	$k_2$ - $k_3$ plane	$\nu_1$ =1	
$k_1 = 0.5$	$k_2$ - $k_3$ plane	$\nu_1' = 0$	
$k_2 = 0.0$	$k_1$ - $k_3$ plane	$\nu_2=1$	
$k_2 = 0.5$	$k_1$ - $k_3$ plane	$\nu_2' = 0$	
$k_3 = 0.0$	$k_1$ - $k_2$ plane	$\nu_3=0$	
$k_3 = 0.5$	$k_1$ - $k_2$ plane	$\nu_3' = 1$	

in both P6/m-Si<sub>6</sub> and P6/m-NaSi<sub>6</sub>, the Fu-Kane parity criterion can be used to easily calculate the  $\mathbb{Z}_2$  topological invariants. We were able to obtain the same  $\mathbb{Z}_2$  topological invariants for both P6/m-Si<sub>6</sub> and P6/m-NaSi<sub>6</sub> by using two different methods, observing hybrid Wannier charge center flows and investigating Fu-Kane parity criterion.  $\nu_0$  is the strong topological index.  $\nu'_n$  (n=1,2,3) are weak topological indices. Table S3 show the example for P6/m-Si<sub>6</sub> at 0 GPa. From the hybrid Wannier charge center flow calculations, we calculated  $\nu'_n$  (n=1,2,3).  $\nu_0$  is obtained by

$$\nu_0 = \nu_1 + \nu_1' = \nu_2 + \nu_2' = \nu_3 + \nu_3' \mod 2, \qquad (S1)$$

and thus we have  $(\nu_0; \nu'_1\nu'_2\nu'_3) = (1;001)$ . Therefore, P6/m-Si<sub>6</sub> at 0 GPa has a strong topological nature. Similarly, we find that P6/m-NaSi<sub>6</sub> at 0 GPa has a strong topological nature.

TABLE S4. Irreducible representation (irrep), point group symmetries, and their eigenvalues of bands at L point.  $C_2$  is two-fold rotation operator with respect to the z-axis. I and  $\sigma_h$  are two-fold inversion and horizontal mirror plane operators, respectively. The highest occupied band is 12th band.

band #	irrep	$C_2$	$\sigma_h$	I
1	$B_u$	-1	+1	-1
2	$A_g$	+1	+1	+1
3	$B_g$	-1	-1	+1
4	$B_u$	-1	+1	-1
5	$A_u$	+1	-1	-1
6	$A_g$	+1	+1	+1
7	$B_g$	-1	-1	+1
8	$A_u$	+1	-1	-1
9	$B_u$	-1	+1	-1
10	$A_g$	+1	+1	+1
11	$A_u$	+1	-1	-1
12	$B_u$	-1	+1	-1
13	$B_g$	-1	-1	+1

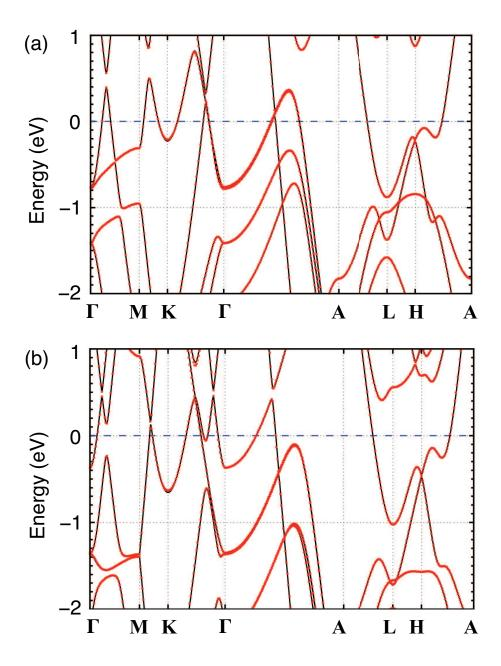


FIG. S4. First-principles bands (solid line) and Wannier bands (red filled circles) of P6/m-Si<sub>6</sub> at (a) 0 GPa and (b) 15 GPa. In the eV energy scale, there are no visible differences between two different bands. Spin-orbit coupling is included.

# IV. Si-Si BOND LENGTHS IN THE SLAB GEOMETRY

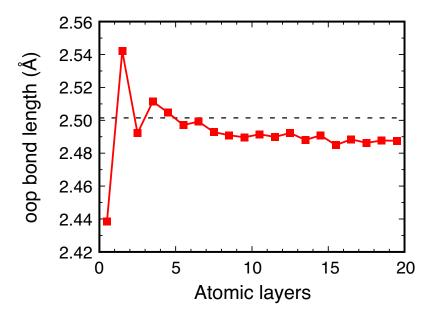


FIG. S5. Si-Si bond lengths, formed in the z direction also denoted by out-of-plane (oop bond lengths) from the hexagonal plane, in the relaxed 40-layer P6/m-Si<sub>6</sub> slab are shown. Position of the surface along the out-of-plane, is set to be zero. Dashed line represents the Si-Si bond length in the unrelaxed slab.

## V. FERMI SURFACES FOR P6/m-Si<sub>6</sub> AND P6/m-NaSi<sub>6</sub>

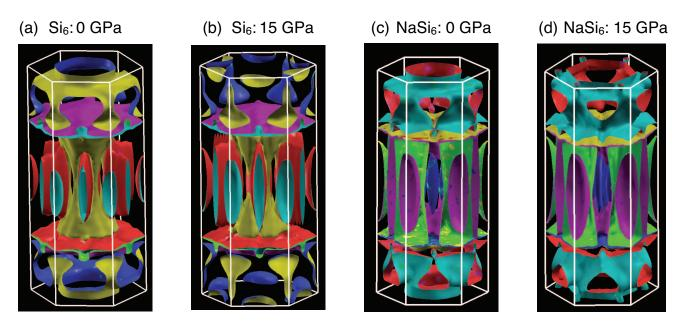


FIG. S6. Electronic band structure obtained from first-principles calculations using DFT. Fermi surfaces of (a) P6/m-Si<sub>6</sub> at 0 GPa, (b) P6/m-Si<sub>6</sub> at 15 GPa, (c) P6/m-NaSi<sub>6</sub> at 0 GPa, and (d) P6/m-NaSi<sub>6</sub> at 150 GPa are shown, respectively. The Fermi surface is the surface of constant energy in the first BZ which separates occupied from unoccupied electron states at zero temperature.